



Measured and modeled ionospheric densities, temperatures, and winds during the international polar year

P. G. Richards,¹ M. J. Nicolls,² C. J. Heinselman,² J. J. Sojka,³ J. M. Holt,⁴ and R. R. Meier¹

Received 6 July 2009; revised 2 September 2009; accepted 25 September 2009; published 22 December 2009.

[1] This paper examines the ability of ionospheric models to reproduce measured electron density, winds, and temperatures during the International Polar Year (IPY) in 2007. The models include the field line interhemispheric plasma (FLIP) model, the international reference ionosphere (IRI) model, and the empirical horizontal neutral wind models (HWM) (HWM93, HWM07). For Poker Flat, Alaska, there is exceptionally good agreement between the FLIP model and measured electron density, winds, and temperatures in equinox and winter. This research shows an interesting post sunset peak in T_e from late fall through early spring that is reproduced by the FLIP model. In June and July the FLIP model underestimates the measured peak electron density by a factor of 2. Although both the data and model show evidence of an F_1 peak near 150 km in summer, the model F_1 peak electron density tends to be larger than the F_2 peak electron density and that is not seen in the data. The summer discrepancy is most likely due to incorrect atomic to molecular neutral density ratios. The FLIP model reproduces the Millstone Hill data well throughout 2007. The IRI model agrees well with the electron density data during the day but overestimates the peak electron density and the height of the peak at night. The equivalent winds from the FLIP model and the winds from the HWM93 model agree well with the measured winds. The HWM07 winds are different from the earlier HWM93 winds at Poker Flat and do not agree as well with the data.

Citation: Richards, P. G., M. J. Nicolls, C. J. Heinselman, J. J. Sojka, J. M. Holt, and R. R. Meier (2009), Measured and modeled ionospheric densities, temperatures, and winds during the international polar year, *J. Geophys. Res.*, *114*, A12317, doi:10.1029/2009JA014625.

1. Introduction

[2] Several incoherent radars were run on a continuous basis during the International Polar Year (IPY). The exceptionally low solar and magnetic activity provides an opportunity to compare ionospheric models with the measurements. In this paper, we concentrate on model-data comparisons for Poker Flat Alaska (65°N, 213°E) for March through December 2007.

[3] The field line interhemispheric plasma (FLIP) model has been developed over a period of more than 30 years [Richards, 2001, 2002, 2004]. It incorporates the basic chemical scheme that was developed from the AE mission but has been updated with more recent information. The FLIP model is generally not run at high latitudes because of the

large uncertainties in particle precipitation, field aligned currents, and plasma convection. The low magnetic activity in 2007 improves the validity of high-latitude FLIP model calculations, but there are still periods where high-latitude processes will invalidate the results. The model uses the Naval Research Laboratory Mass Spectrometer Incoherent Scatter (MSIS) Radar Extended (NRLMSISE-00) empirical approach to provide neutral densities and temperatures of the thermosphere.

[4] The standard solar irradiances come from the EUVAC model [Richards *et al.*, 1994], which drives the computation of photoionization rates. Photoelectron fluxes require a finer wavelength grid and are calculated separately using the High Resolution EUV model for aeronomic calculations (HEUVAC) model [Richards *et al.*, 2006]. HEUVAC retains the basic EUVAC but extends the spectrum below 50 Å and has a finer wavelength grid. For this paper we have also used the Thermosphere Ionosphere Mesosphere Energetics and Dynamics (TIMED) Solar EUV Experiment (SEE) EUV irradiances that are available throughout 2007 [Woods *et al.*, 2008]. To facilitate solar cycle variations, we have created a model for the SEE irradiances, which are produced on a 1 nm wavelength grid, on the same 37 wavelength bins that are used in the EUVAC model.

[5] For this study, the chemical reaction rates of Fox and Sung [2001] have been adopted. Two of these reaction rates

¹Department of Physics and Astronomy, George Mason University, Fairfax, Virginia, USA.

²Center for Geospace Studies, SRI International, Menlo Park, California, USA.

³Center for Atmospheric and Space Sciences, Utah State University, Logan, Utah, USA.

⁴Haystack Observatory, Massachusetts Institute of Technology, Westford, Massachusetts, USA.

were reparameterized to better fit the laboratory data of *Li et al.* [1997]. The reaction rate for the $O^+(^2D) + N_2 \rightarrow N_2^+ + O$ is well fit by the function $1.5 \times 10^{-10}(300/Ti)^{-0.55} \text{ cm}^3 \text{ s}^{-1}$, and the reaction rate for the $O^+(^2P) + N_2 \rightarrow N_2^+ + O$ is well fit by the function $2.0 \times 10^{-10}(300/Ti)^{-0.55} \text{ cm}^3 \text{ s}^{-1}$. $O^+(^2D)$ and $O^+(^2P)$ can be significant sources of the ground state $O^+(^4S)$ above 250 km under some conditions.

[6] The main $O^+(^4S)$ loss rates are $O^+(^4S) + N_2 \rightarrow NO^+ + N$ and $O^+(^4S) + O_2 \rightarrow O_2^+ + O$. Some researchers have adopted the latest laboratory measurements of *Hierl et al.* [1997] for these reactions rates. These rates agree well with a number of other measurements below 1000°K but are much larger at higher temperatures because of vibrational excitation as noted by the authors. Although N_2 is vibrationally excited in the thermosphere, the distribution will not be the same as in the laboratory. So the laboratory rates are not appropriate for the ionosphere. Vibrational excitation is important because it can lower the electron density by accelerating the $O^+ + N_2$ reaction rate. The FLIP model solves for vibrationally excited nitrogen (N_2v) and the O^+ loss rate can increase by more than a factor of 2 at solar maximum. It is a small effect at solar minimum decreasing the model N_mF_2 by about 15% during 2007. For the present study, the temperature variation of the $O^+(^4S) + N_2 \rightarrow NO^+ + N$ reaction rate is taken from *St. Maurice and Torr* [1978], and the rate is normalized to the laboratory measurements at 900°K. The temperature variation of the $O^+(^4S) + O_2 \rightarrow O_2^+ + O$ reaction rate is taken from *McFarland et al.* [1973]. At solar minimum, the FLIP model N_2 and O_2 loss rates are approximately equal near 250 km altitude.

[7] The primary heat source for thermal electrons is the photoelectron flux, which is calculated by the FLIP model. There is an additional important source of electron heating from electron quenching of $N(^2D)$ [*Richards*, 1986]. The FLIP model electron-ion cooling rate is from *Itikawa* [1975]. The electron-neutral and ion-neutral cooling rates are from *Schunk and Nagy* [1978]. Heat flow from the plasmasphere is an important nonlocal heat source that can persist after sunset. Photoelectron escape above about 300 km is the sole source of plasmaspheric heating in the model. The closed field lines in the FLIP model means that both local and conjugate hemispheres can contribute to plasmaspheric heating. For Poker Flat, the conjugate hemisphere can remain sunlit all day in winter. We emphasize that the model plasmaspheric heating is entirely due to Coulomb interactions by photoelectrons escaping from both hemispheres. No additional plasmaspheric heat source was assumed.

[8] The international reference ionosphere (IRI) model is an empirical model that is known to represent the median state of the ionosphere very well [*Bilitza et al.*, 1993; *Bilitza*, 2001]. IRI is an international project sponsored by the Committee on Space Research and the International Union of Radio Science. The IRI values presented in this paper were obtained from the version on the community coordinated modeling center Web site.

[9] To successfully capture the F_2 region ionosphere electron density, it is necessary to first accurately model the variation of the measured height of the peak electron density (h_mF_2), which is primarily influenced by the neutral wind component in the magnetic meridian. The FLIP model has the ability to accurately reproduce h_mF_2 by automatically adjusting the neutral winds as it steps in time using the

technique of *Richards* [1991]. These are termed equivalent winds because they may contain an electric field contribution. However, numerous tests have shown that these equivalent winds agree well with actual winds from other techniques [e.g., *Dyson et al.*, 1997; *Buonsanto et al.*, 1997a, 1997b]. In any case, the inclusion of electric fields is a bonus because they are also necessary to accurately model the ionosphere. The FLIP model also uses winds from the HWM93 and HWM07 horizontal wind models [*Hedin et al.*, 1996; *Drob et al.*, 2008] in this paper.

[10] Independent of the source of winds there are two other possible sources of error that are related to each other in the sense that they both affect the momentum transfer between ions and neutrals. These are the uncertainty in the atomic oxygen density and in the O^+ -O collision frequency. Early comparison of winds determined from optical measurements with winds inferred from incoherent scatter radars led to the adoption of the so-called Burnside factor of 1.7 by the aeronomy community [*Salah*, 1993]. The Burnside factor is a multiplicative factor for the collision frequency of *Schunk and Walker* [1973]. More recent determinations from theoretical calculations and from evaluation of the optical and radar data point to a multiplicative factor of 1.2 to 1.4. *Buonsanto et al.* [1997a, 1997b] reviewed the collision frequency problem. Neither the winds from incoherent scatter radars nor the equivalent winds from h_mF_2 can distinguish between errors in the model atomic oxygen density and errors in the collision frequency.

[11] We have adopted a Burnside factor of 1.3 to multiply the O^+ -O collision frequency for all calculations in this paper. This could be considered a problem for the h_mF_2 calculated using the HWM wind models because these models are partly based on old Poker Flat and Millstone Hill radar data that were analyzed using a Burnside factor of 1.7. However, our calculations indicate that the two different Burnside factors do not affect the model results very much. For example, the lower Burnside factor causes h_mF_2 to be 10–15 km lower at night when the FLIP model uses the HWM winds.

2. Radar Data

[12] The Poker Flat Advanced Modular Incoherent Scatter Radar (PFISR) is located at the Poker Flat Research Range near Fairbanks, Alaska. PFISR is the first incoherent scatter radar (ISR) that uses phased array technology to steer on a pulse-to-pulse basis over a limited field of view [*Heinselmann and Nicolls*, 2008]. Furthermore, the modern design of the system allows it to be operated remotely and continuously.

[13] The operating mode for the IPY and normal background monitoring consists of low-duty cycle (~1%) transmissions and one to four look directions, including one beam directed up the local magnetic field line (data from which are used in this study). Transmissions for the IPY mode consist of a 480 μs (72 km) long pulse for F region studies interleaved with a 4.5 km resolution alternating code for E region studies. Data are typically processed at 15 min integration periods because of the low-duty cycle, although higher time resolutions are available during high-SNR conditions. The normal analysis consists of fits for the electron density and temperature as well as the ion temperature and line-of-sight speed. Electron densities are calibrated using daytime measurements of the plasma line. For more details on the IPY

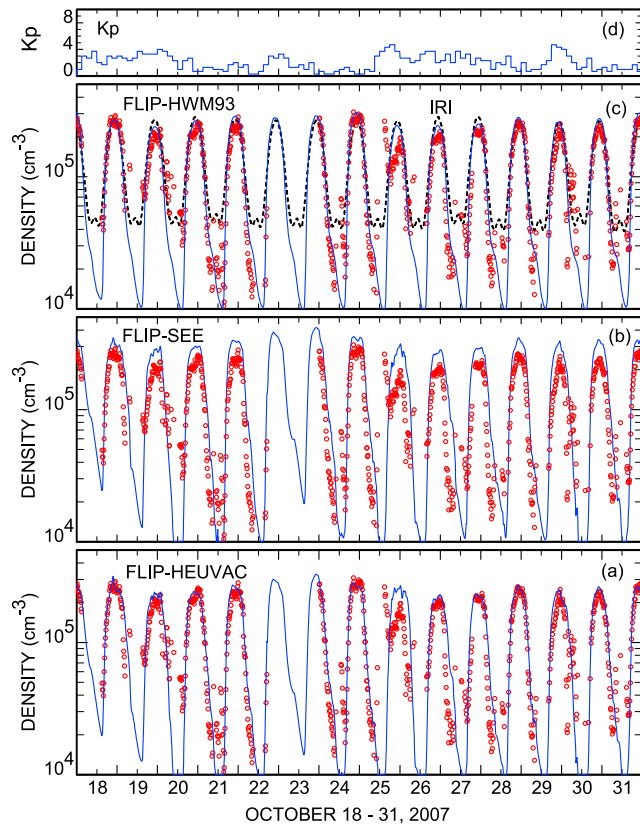


Figure 1. Comparison of different model calculations (lines) with the measured N_mF_2 (circles) 18–31 October 2007 (long tick marks are for 0000 UT, \sim 1400 LT). (a) The model calculation using the HEUVAC model solar irradiances when the measured h_mF_2 is used to provide the equivalent wind. (b) The model calculation using the SEE model solar irradiance when the measured h_mF_2 is used to provide the equivalent wind. (c) The model calculation using the HEUVAC model solar irradiance and the HWM93 model (solid line). The dashed line shows the IRI N_mF_2 . (d) The K_p index.

operations, the reader is referred to *Sojka et al.* [2009]. An independent ion composition estimate is needed to determine temperatures in the lower F region from incoherent scatter measurements (e.g., see *Aponte et al.* [2007] for details about this issue). For this purpose, a fixed molecular ion fraction profile has been used, based on the formulation of *Evans and Oliver* [1972] and *Oliver* [1975], which yields a 50% transition altitude around 160 km altitude. This procedure is a source of uncertainty for the temperatures in the transition region from molecular ions to O^+ ions. The FLIP model 50% transition altitudes, which are near 200 km, were used in the fitting process for the altitude profiles in this paper. This resulted in more physically reasonable altitude profiles without discontinuities in the measured temperatures.

[14] Second-order products such as h_mF_2 and N_mF_2 were derived from the data when densities were sufficiently high and when the layer profile was suitable for the determination of those parameters (e.g., during times of particle precipitation, this was not in general possible). The h_mF_2 and N_mF_2 values were found by applying polynomial fits to the electron density profiles near the peak of the layer.

[15] Winds along the magnetic meridian were also derived from F region field-aligned motions using techniques standard for midlatitude observatories [e.g., *Salah and Holt*, 1974; *Buonsanto and Witasse*, 1999; *Aponte et al.*, 2005]. This approach corrects the field-aligned ion motion for nominal ambipolar diffusion effects (using, in our case, the NRLMSISE-00 background neutral atmosphere model) and interprets the remaining component of the motion as due to the projection of the magnetically southward wind. The magnetic dip angle at PFISR’s location is $\sim 77.5^\circ$ (declination $\sim 20^\circ$) which makes this technique error prone and difficult (for example, a 100 m s^{-1} neutral wind will result in $\sim 20 \text{ m s}^{-1}$ field-aligned motion, and typical line-of-sight velocity errors are in the range of $10\text{--}20 \text{ m s}^{-1}$). In addition, enhanced diffusion, for example, due to ion upflow driven by auroral processes, will bias these estimates. Nevertheless, as we will show, reasonable estimates of the winds can be obtained but must be interpreted cautiously.

3. Results

[16] Model calculations were compared to PFISR data from the beginning of measurements in March through December 2007. Except in June and July where the FLIP model daytime N_mF_2 is generally a factor of 2 too low, all the model calculations give very good agreement for densities, winds, and temperatures for 2007. Results are presented for 18–31 October 2007, which is representative of the agreement between model and data for months other than June and July. The summer calculations are for 10–24 June and 25 July to 6 August, which represent all summer model data comparisons.

[17] The Millstone Hill radar was operated for thirty-three 1–3 day periods during 2007. We performed calculations using the HEUVAC solar irradiances for 20–23 January, 29–30 March, 20–22 June, and 11–14 September 2007. The agreement between the modeled and measured daytime electron density and temperature is excellent in all four cases.

[18] Plasma convection is normally a complicating factor for models at high latitudes. Some convection periods can be identified in the 2007 radar data because the ion temperature is elevated due to frictional heating. These convection periods appear to have little effect on the measured electron densities and temperatures. Modeling convection is very difficult because it requires specifying the convection pattern over the entire high-latitude region. The FLIP model is capable of incorporating electric field drifts [*Richards et al.*, 2000] but they have not been included in this paper.

3.1. October 2007 N_mF_2

[19] Figure 1 shows comparisons of different model calculations (lines) with the measured N_mF_2 (circles) for 18–31 October 2007 (long tick marks are for 0000 UT, 1400 LT). Figure 1a shows the FLIP model calculation using the HEUVAC model solar irradiances when the measured h_mF_2 is used to provide the equivalent wind. Note that h_mF_2 data gaps were filled in using the IRI h_mF_2 if they were more than 1 h. During the daytime, the agreement between the model and data is excellent using the HEUVAC irradiances, even to the extent of reproducing the observed response to magnetic activity. The magnetic activity changes in the model are the result of changes in the neutral densities from the

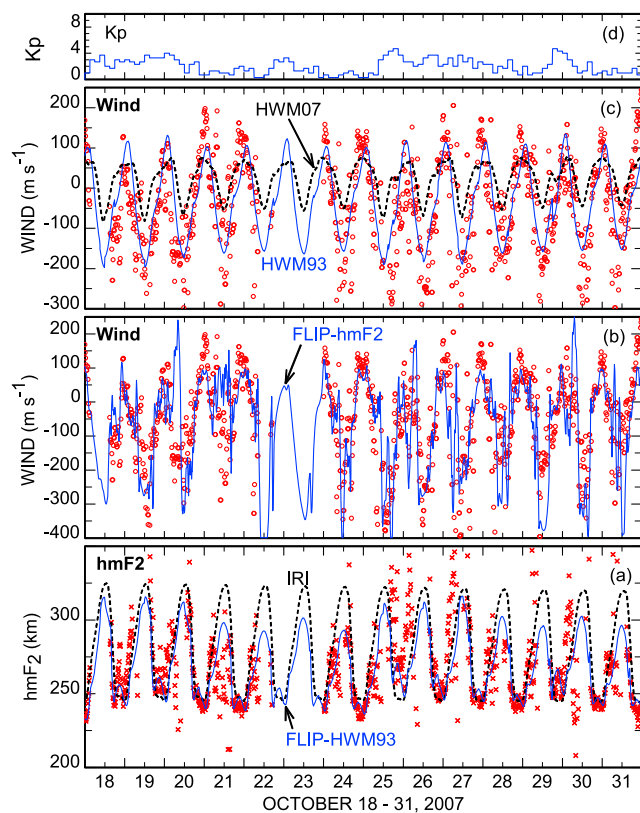


Figure 2. Comparison of different model calculations (lines) with the measured $h_m F_2$ (crosses) and winds (circles) for 18–31 October 2007 (long tick marks are for 0000 UT, ~ 1400 LT). (a) The model $h_m F_2$ calculation using the HWM93 model winds. The dashed line Figure 2a shows the IRI $h_m F_2$. (b) The model equivalent wind calculation using the measured $h_m F_2$ (solid line). (c) The HWM93 (solid line) and HWM07 (dashed line) model winds compared to the data (solid line). The winds are for 276 km altitude and poleward winds are positive. (d) The K_p index.

NRLMSISE-00 model. The top panel shows the K_p magnetic activity index for the 18–31 October period. The nighttime is notoriously difficult to model because small errors in winds or loss rates can accumulate to produce large model errors over several hours. However, even the nighttime densities are well modeled for 18–31 October 2007. The nighttime agreement is also very good at other times in 2007, except for summer.

[20] Figure 1b shows the FLIP model $N_m F_2$ when using the SEE solar irradiances. In this case, the model $N_m F_2$ is 15–20% higher than when using HEUVAC but still in good agreement with the data. Figure 1c shows that there is also good agreement when the FLIP model calculation uses the HEUVAC solar irradiances together with the HWM93 wind model (solid line). The IRI model (dashed line) gives very good agreement during the day but is generally a factor of 2 too high at night.

3.2. October 2007 $h_m F_2$ and Winds

[21] Figure 2 shows a comparison of different model calculations (lines) with the measured $h_m F_2$ (crosses) and winds (circles) for 18–31 October 2007. Figure 2a shows that

the FLIP model $h_m F_2$ calculated with the HWM93 model winds agrees well with the data in daytime but underestimates the height at night. Increasing the Burnside factor to 1.7 improves the nighttime agreement by increasing the height by about 15 km. The dashed line in Figure 2a shows the IRI $h_m F_2$, and it also agrees well with the data. Figure 2b compares the radar winds with the FLIP model equivalent winds calculation using the measured $h_m F_2$ (solid line). As expected, the winds tend to be poleward (northward) during the day and equatorward (southward) at night. Poleward neutral winds are positive.

[22] The measured winds are presented for a fixed altitude of 276 km, whereas the equivalent winds are at $h_m F_2$. The altitude difference between $h_m F_2$ and 276 km is not expected to be significant because the altitude variations of the winds are thought to be small above 200 km under normal circumstances. Note that both the model and data values have been smoothed slightly using a running mean with a 1 h window to make it easier to compare them. It is important to look at the $h_m F_2$ in Figure 2a when comparing the modeled and measured winds because there are periods where the $h_m F_2$ data coverage is sparse, especially at night, and the model winds actually come from the IRI $h_m F_2$ at these times. The FLIP model equivalent winds are the most reliable during daytime where the agreement is very good. For example, witness the good daytime agreement on 20–21 and 25–26 October. The nighttime equivalent winds are less reliable because of the sparseness of the $h_m F_2$ data. Nevertheless, the general agreement with the radar winds indicates that the large measured winds are consistent with the variations in $h_m F_2$. Some of the differences between the winds in Figure 2b could be the result of electric field drifts being included in the equivalent winds. The equivalent winds are also sensitive to errors in the measured $h_m F_2$.

[23] Figure 2c shows that the HWM93 model winds (solid line) also compare well to the data. This explains why there is good agreement between measured and modeled $N_m F_2$ and $h_m F_2$ when the FLIP model uses the HWM93 model winds with the HEUVAC solar irradiance model. The HWM07 winds (dashed line) do not fit the data as well as the HWM93 winds for this period.

[24] Previously, it was thought that the latitude of Poker Flat was too high to determine equivalent winds because the calculation of equivalent winds from $h_m F_2$ is sensitive to the dip angle. The method does not work at equatorial latitudes where the field lines are horizontal or at very high latitudes where the field lines are vertical. The dip angle at Poker Flat is 77.5° . The accuracy of the derivation of the horizontal winds from the incoherent scatter radar suffers from the same dip angle problem. The good agreement in Figure 2b indicates that the equivalent winds are at least as good as the radar winds at high latitudes during magnetically quiet times.

3.3. October 2007 Electron and Ion Temperatures

[25] Figure 3 shows a comparison of different model calculations (lines) with the measured ion and electron temperatures (circles) for 18–31 October 2007. The bottom panel shows the model electron temperature calculation using HEUVAC (solid line) and SEE (dashed line) solar EUV irradiances. The agreement between the calculated and measured electron temperatures is very good, especially given the

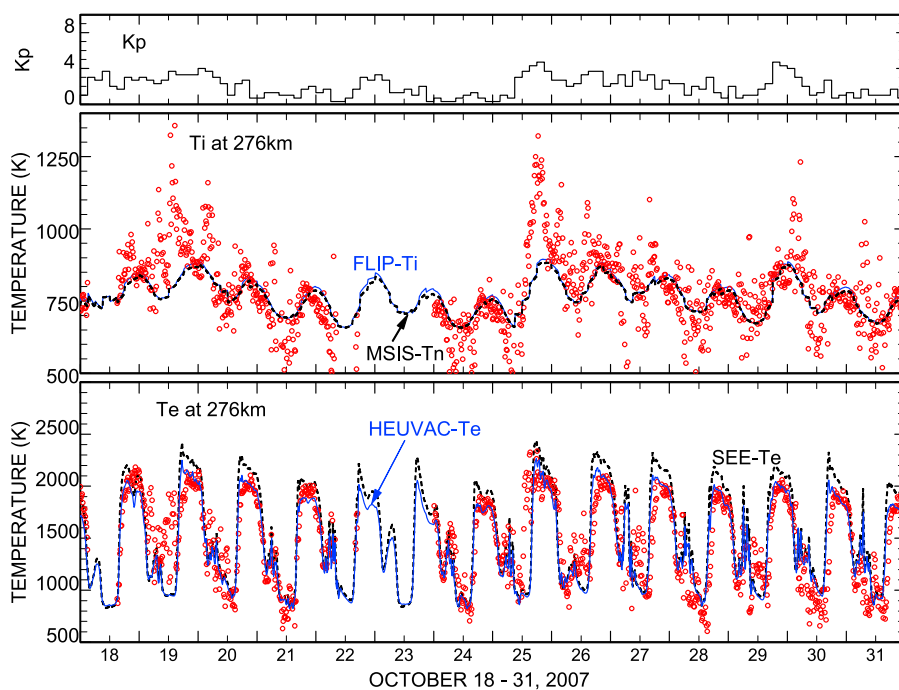


Figure 3. Comparison of different model calculations (lines) with the measured ion and electron temperatures (circles) for 18–31 October 2007 (long tick marks are for 0000 UT, ~1400 LT). (bottom) The model electron temperature calculation using HEUVAC (solid line) and SEE (dashed line) solar EUV irradiances. (middle) The model ion temperature calculation using the HEUVAC solar EUV irradiances (solid line) and the MSIS model neutral temperature (dashed line). (top) The K_p index.

uncertainty in heat flow from the plasmasphere. Because the daytime $N_m F_2$ is larger when using the SEE irradiances, we would expect the corresponding electron temperatures to be smaller than those from the HEUVAC model. However, the SEE calculated temperatures are actually slightly higher than

the HEUVAC-calculated temperatures because there are more photons between 25 and 40 nm that produce larger photoelectron fluxes. The middle panel of Figure 3 shows the model ion temperature calculation using the HEUVAC solar EUV irradiances (solid line). The daytime model ion temper-

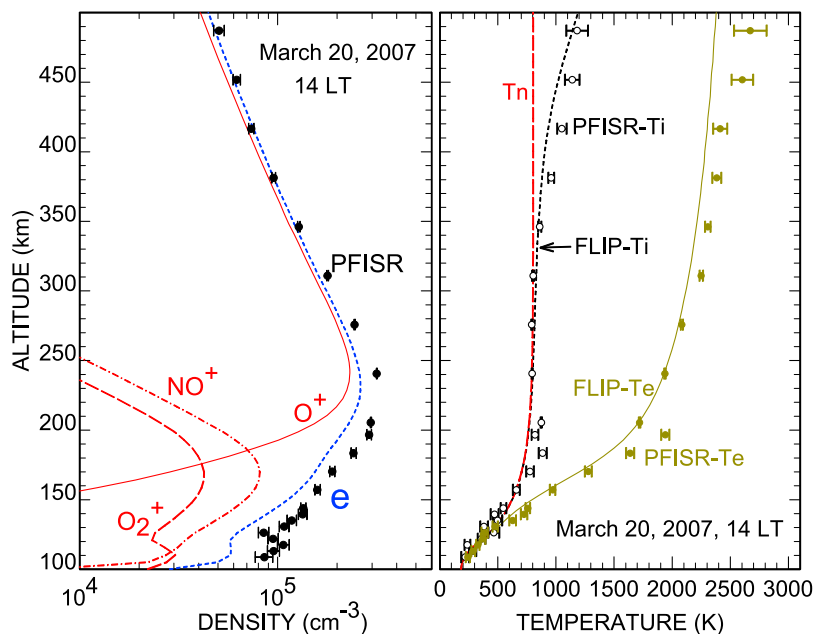


Figure 4. Comparison of altitude profiles of modeled (lines) and measured electron density (solid circles), electron temperature (solid circles), and ion temperature (open circles) for 20 March 2007. The model ion densities are also shown. The model calculations used HEUVAC solar EUV irradiances.

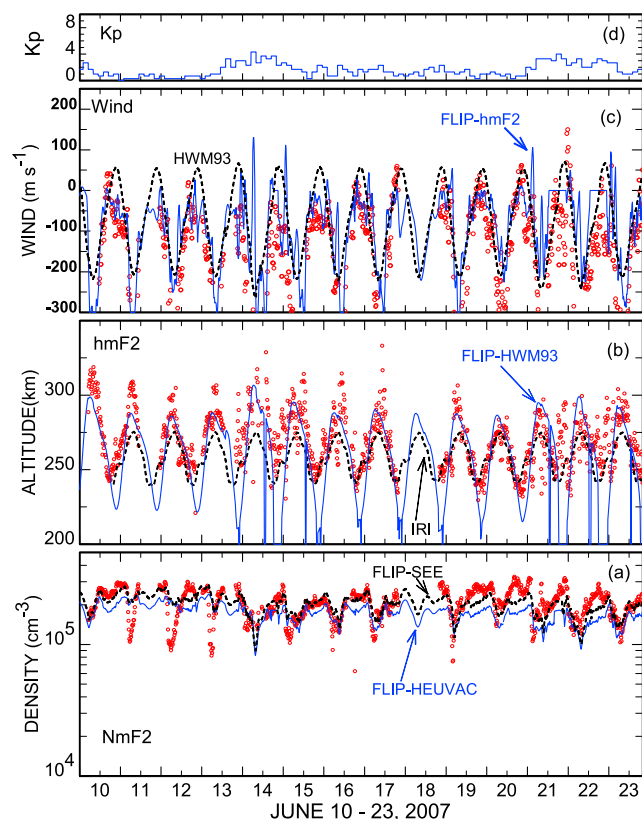


Figure 5. Comparison of different model calculations (lines) with the measured N_mF_2 , h_mF_2 , and winds (circles) for 10–23 June 2007 (long tick marks are for 0000 UT, ~ 1400 LT). (a) The calculated N_mF_2 using HEUVAC (solid line) and SEE (dashed line) solar irradiances. (b) The model h_mF_2 calculation using the HWM93 model winds (solid line) and the IRI h_mF_2 (dashed line). (c) Comparison of the model equivalent wind calculation using the measured h_mF_2 (solid line) and the HWM93 model winds (dashed line) with the radar winds. (d) The Kp index.

ature is typically about 15°K higher than the NRLMSISE-00 neutral temperature. The agreement between the modeled and measured ion temperatures is generally very good. The high ion temperatures on 19, 25, and 30 October appear to be associated with increases in Kp and are probably the result of frictional heating from ion convection since the electron density and electron temperature are unaffected.

[26] There is a particularly interesting electron temperature peak in the model and data after local sunset near 0700 UT (2100 LT) that is well captured by the model on most days. This post sunset peak occurs, despite absence of local electron heating, because there remains a significant heat flux from the plasmasphere while the rapid decrease in electron density causes the electron cooling rate to decrease substantially. The electron temperature eventually decreases again as the plasmaspheric heat flux decreases. In the model, this post sunset temperature peak occurs because the conjugate point is still sunlit. This also explains why the peak does not occur at equinox or summer when the conjugate point is not sunlit after local sunset. The existence of the temperature peak supports the assumption that the field line is closed at Poker Flat at these times.

3.4. March Density and Temperature Profiles

[27] Figure 4 shows a comparison of altitude profiles of modeled (lines) and measured electron density (solid circles), electron temperature (solid circles) and ion temperature (open circles) for 20 March 2007. The model calculations used HEUVAC solar EUV irradiances. As in October, there is excellent agreement between the modeled and measured peak electron density. There is also good agreement at other altitudes. The electron and ion temperatures are also well modeled at all altitudes. Note that a molecular ion fraction profile with a nominal 50% transition altitude of ~ 190 km, obtained from the FLIP model, was used for fitting the IS data. Sources of error in the radar analysis include range smearing of the long, uncoded pulse as well as the effects of molecular ion composition, as discussed in section 2.

3.5. June 2007 N_mF_2 , h_mF_2 , and Neutral Winds

[28] Figure 5 shows a comparison of different model calculations (lines) with the measured N_mF_2 , h_mF_2 , and neutral winds (circles) for 10–23 June 2007. Figure 5a shows the measured and modeled N_mF_2 using HEUVAC (solid line) and SEE (dashed line) solar irradiances. The modeled and measured N_mF_2 has much less diurnal variation in summer than equinox and winter. The SEE irradiances give the best agreement with the data, but neither set of irradiances produce particularly good agreement with the measured N_mF_2 , which has a much greater diurnal variation. The IRI model (not shown) gives good agreement with the measured N_mF_2 during the daytime but also underestimates the diurnal variation.

[29] The dashed line in Figure 5b shows the IRI h_mF_2 , which agrees well in the daytime but underestimates the nighttime by about 50 km. The solid line in Figure 5b shows the FLIP model h_mF_2 calculation using the HWM93 model winds. There is satisfactory agreement during the night but the model h_mF_2 from the HWM93 winds are too low during the daytime because the maximum electron density occurs below 200 km. In other words, the F_1 density is larger than the F_2 density. The solar zenith angle hardly gets larger than 90° in summer at Poker Flat, but this is sufficient to decrease the F_1 region density relative to the F_2 region density so that the model peak electron density stays well above 200 km for the larger solar zenith angles. The measured maximum daytime N_mF_2 shows little variation between summer and other times. Taking into account the lack of change in the measured daytime h_mF_2 and the SEE irradiances during 2007, the low daytime model densities are most likely due to too low NRLMSISE-00 model atomic oxygen to molecular density ratio. The FLIP model N_2 and O_2 losses are approximately equal at h_mF_2 .

[30] Figure 5c shows the measured wind (circles), HWM93 winds (dashed line) and the model equivalent wind calculation using the measured h_mF_2 (solid line) for June 2007. The HWM07 agree reasonably well with the HWM93 winds and are not shown. There is good agreement between the winds on 10–12 and 15–17 June. The histogram like features in the equivalent winds on days 13, 20, and 21 arise because the model is not able to maintain the peak density above 200 km. When this happens, the model wind is set to 0 because there is no model h_mF_2 from which to calculate the equivalent wind. This further supports the idea that the NRLMSISE-00 O to N_2 ratio is too small in summer at Poker Flat.

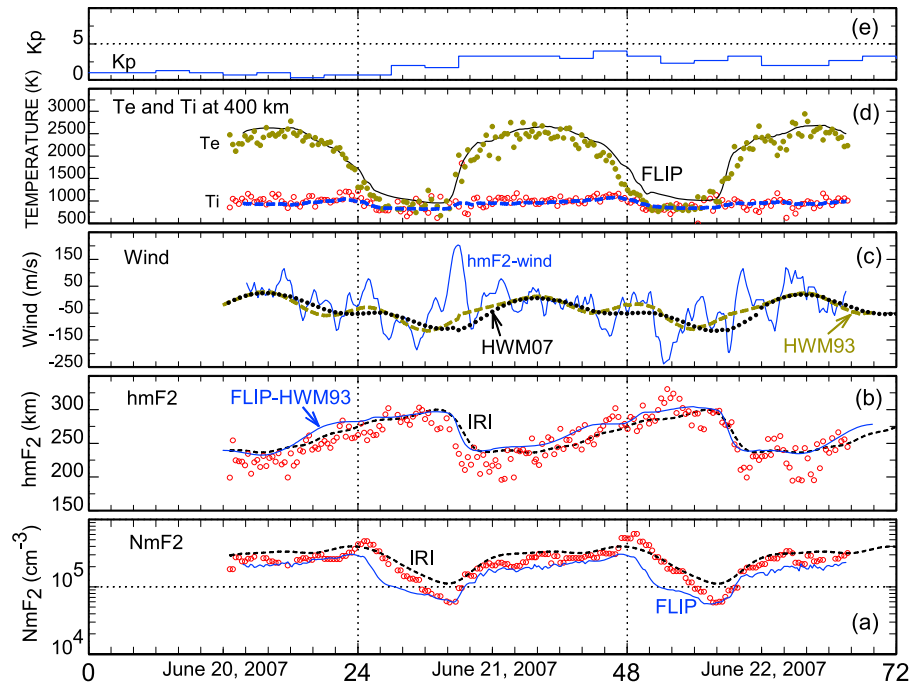


Figure 6. Comparison of different model calculations (lines) with the measured N_mF_2 , h_mF_2 , winds, and temperatures (symbols) for 20–21 June 2007 at Millstone Hill (43°N, 285°E). The vertical lines are for 0000 UT, \sim 1900 LT. (a) The IRI model (dashed line) and calculated N_mF_2 using the HEUVAC (solid line) solar irradiances. (b) The h_mF_2 calculated using HWM93 winds (solid line) and the IRI h_mF_2 (dashed line). (c) Comparison of the model equivalent wind calculation using the measured h_mF_2 (solid line) with the HWM93 model (dashed line) and the HWM07 model (dotted line). (d) The calculated electron (solid line) and ion (dashed line) temperatures and measured electron (solid circles) and ion (open circles) temperatures. (e) The K_p index.

[31] The Poker Flat discrepancy does not appear to be related to the solar EUV irradiances because the FLIP model produces very good agreement with ISR data from Millstone Hill and several Australian ionosonde stations at the June solstice using the HEUVAC irradiances. Figure 6a shows that there is excellent agreement between the modeled (solid line) and measured (open circles) N_mF_2 at Millstone Hill during the daytime for 20–23 June which is a period of large discrepancy at Poker Flat as shown in Figure 5. The N_mF_2 agreement at Millstone Hill deteriorates after sunset because the model does not show the post sunset density enhancement that is evident in the measurement. The IRI N_mF_2 (dashed line) is higher than the measured N_mF_2 , but the agreement is still very good. Figure 6b shows that the IRI model (dashed line) and the HWM winds reproduce the measured h_mF_2 well. Figure 6c shows the FLIP model equivalent winds (solid line) compared to the HWM93 (dashed line), and HWM07 (dotted line) model winds. There is good agreement between the two HWM model winds for these conditions. The equivalent winds are more variable than the HWM winds, but the overall magnitude and diurnal variation is similar. The equivalent winds are more reliable at Millstone Hill than Poker Flat because the dip angle is 69° and there are no contaminating auroral processes. As a result, the Millstone Hill equivalent winds are much smaller and less variable than the PFISR winds. The wave like variability is not unusual for Millstone Hill. Figure 6d shows that the FLIP model electron and ion temperatures are in excellent agreement with the measurements at 400 km where the major heat source for thermal

electrons is heat conduction from the plasmasphere due to Coulomb interactions of thermal electrons with photoelectrons escaping from both hemispheres. No additional ad hoc plasmaspheric heat source was assumed in the model.

3.6. June 2007 Electron and Ion Temperatures

[32] Figure 7 shows a comparison of different model calculations (lines) with the measured ion and electron temperatures (circles) for 10–23 June 2007 for Poker Flat. The bottom panel shows the model electron temperature calculation using HEUVAC (solid line) and SEE (dashed line) solar EUV irradiances. Both of the calculated electron temperatures overestimate the measured electron temperature during the daytime. Given that the calculated daytime densities are smaller than the measured densities the higher model electron temperatures are to be expected. However, some of the discrepancy could be attributed to uncertainty in heat flow from the plasmasphere. The middle panel of Figure 7 shows that the model ion temperature calculation using the HEUVAC solar EUV irradiances (solid line) agrees well with the data. The daytime model ion temperature is typically about 15°K higher than the NRLMSISE-00 neutral temperature.

3.7. June Density and Temperature Profiles

[33] Figure 8 shows a comparison of altitude profiles of modeled (lines) and measured electron density (solid circles), electron temperature (solid circles) and ion temperature (open circles) for 20 June 2007. The model calculations used

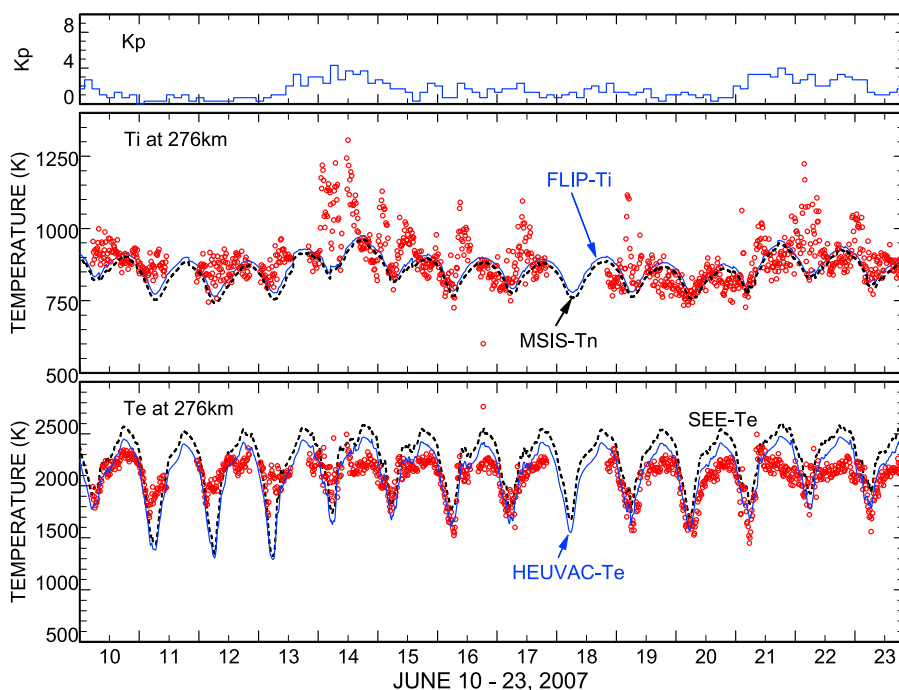


Figure 7. Comparison of different model calculations (lines) with the measured ion and electron temperatures (circles) for 10–23 June 2007 (long tick marks are for 0000 UT, ~1400 LT). (bottom) The model electron temperature calculation using HEUVAC (solid line) and SEE (dashed line) solar EUV irradiances. (middle) The model ion temperature calculation using the HEUVAC solar EUV irradiances. The dashed line shows the MSIS model neutral temperature. (top) The K_p index.

HEUVAC solar EUV irradiances. There is reasonably good agreement between measured and modeled electron density for this day. However, the altitude profiles differ in shape. While both density profiles show F_1 and F_2 peaks, the measured maximum density is near 250 km while the modeled

maximum density is near 150 km. The model does have a very weak F_2 peak near where the measured density peaks. The model densities agree well with the measurements below 200 km. As in March, there is very good agreement between modeled and measured ion and electron temperatures at all

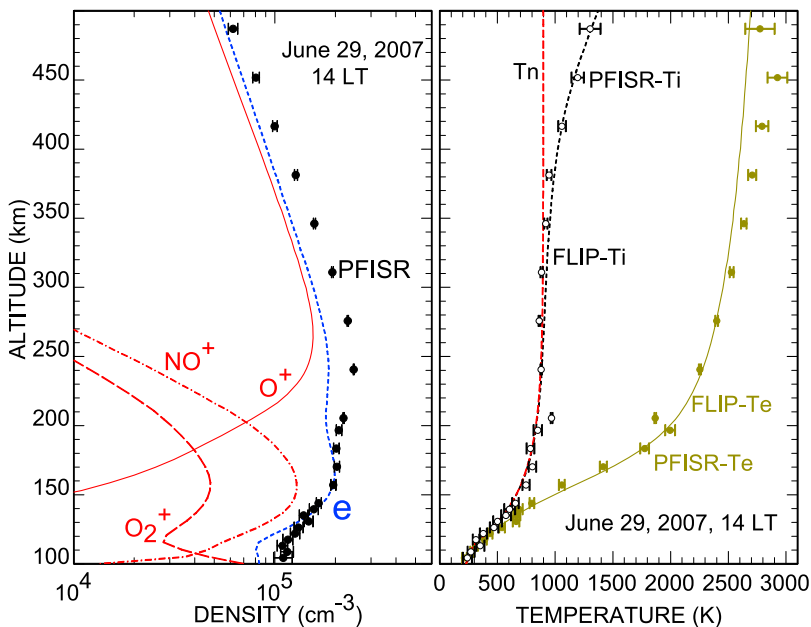


Figure 8. Comparison of altitude profiles of modeled (lines) and measured electron density (solid circles), electron temperature (solid circles), and ion temperature (open circles) for 29 June 2007. The model ion densities are also shown. The model calculations used HEUVAC solar EUV irradiances.

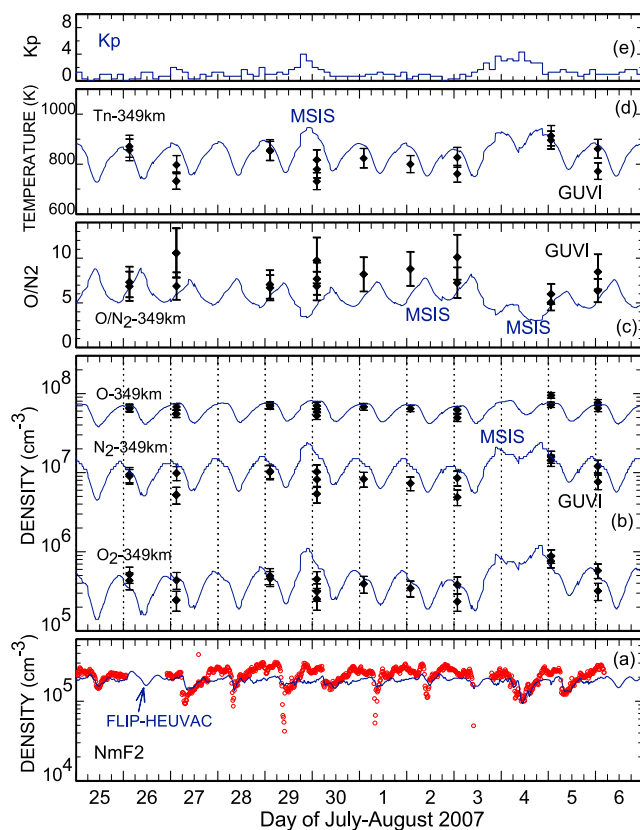


Figure 9. Comparison of densities and temperatures for 25 July to 6 August 2007. Long tick marks are for 0000 UT, ~ 1400 LT. The lines show model values while diamonds with error bars show GUVI data. NRLMSISE-00 and GUVI values are for at 349 km altitude. (a) The radar $N_m F_2$ (circles) together with the FLIP model calculated $N_m F_2$ using HEUVAC solar irradiances. (b) The GUVI and NRLMSISE-00 neutral densities. (c) The GUVI and NRLMSISE-00 O to N_2 density ratios. (d) GUVI and NRLMSISE-00 neutral temperatures. (e) The K_p index.

altitudes. The PFISR data analysis used a molecular ion transition altitude of ~ 210 km, as predicted by the FLIP model.

3.8. July–August 2007 Densities and Temperatures

[34] To further investigate the summer $N_m F_2$ discrepancy, we have examined neutral densities and temperatures from the Global Ultraviolet Imager (GUVI) on board the TIMED satellite. The TIMED satellite was launched on 7 December 2001 into a 630 km circular orbit with an inclination of 74.1° . The TIMED orbit precesses at a rate such that the angle between the Earth-Sun vector and the orbital plane (beta angle) passes through 0 every 120 days. As a result, the combined ascending and descending orbital passes allow GUVI to sample all local solar times every 60 days. Height profiles of the O, N_2 , and O_2 densities and temperature are retrieved from limb altitude profiles of the atomic oxygen 135.6 nm and molecular nitrogen Lyman-Birge-Hopfield (LBH) band radiances using procedures described by Emmert *et al.* [2006]. The latest version of the GUVI limb database (version 9) has significant improvements. Most important is the inclusion of both LBH short wavelength

(141–152.8 nm) and long wavelength (167.2–181.2 nm) data, which greatly improves the accuracy of the O_2 retrievals. Version 9 GUVI limb data can be obtained via the Virtual Ionosphere Thermosphere Mesosphere Observatory Web site (available at <http://vitmo.jhuapl.edu/>).

[35] There are no GUVI data for the 10–23 June 2007 period because the look angle precluded measurements to high latitudes in the Northern Hemisphere. However, there are data for 25 July to 6 August 2007 when there is still an $N_m F_2$ discrepancy. Figure 9 shows this $N_m F_2$ discrepancy along with the neutral densities and temperatures. The GUVI measurements were obtained just after 0000 UT. The local time of the measurements ranged from ~ 1700 on 26 July to ~ 1500 on 6 August. The error bars on the GUVI data are from counting statistics and do not include systematic uncertainties, which are currently being evaluated. Figure 9b shows that there is fair agreement between the NRLMSISE-00 and GUVI O and O_2 densities but the GUVI N_2 densities are substantially lower. This translates into the GUVI O to N_2 density ratios being substantially higher than the NRLMSISE-00 ratios as shown in Figure 9c. The lower GUVI N_2 densities appear to be associated with lower neutral temperatures as shown in Figure 9d. Caution is needed in interpreting the GUVI data at high latitudes because auroral emissions can adversely affect the retrieval procedure. However, Figure 9e shows that, except for 4 August, the magnetic activity was very low during this period. The GUVI data support the likelihood that the summer $N_m F_2$ discrepancy is due to the NRLMSISE-00 neutral temperatures and N_2 densities being too high. This is unusual in that our numerous previous calculations have found that the NRLMSISE-00 neutral densities generally produce good agreement between the daytime modeled and measured $N_m F_2$ at midlatitudes.

4. Conclusions

[36] This paper shows that the basic ionospheric chemistry, dynamics, and energetics are generally well represented by the FLIP ionosphere model using standard neutral densities, reaction rates, and solar EUV irradiances. However, the model does not reproduce the June–July electron density at Poker Flat very well, even though it does produce good agreement at Millstone Hill. There is a fundamental difference between the modeled and measured altitude density profiles in June–July at Poker Flat. That is, the measured daytime electron density peaks well above 200 km while the model has a strong tendency to peak below 200 km. Auroral processes that have not been included in the FLIP model calculations probably account for some differences between the model and data. These auroral processes include energetic particle precipitation, field-aligned currents, and ion convection. However, these processes tend to be spasmodic in time and are therefore not likely to account for extended periods of disagreement between model and data. The most likely explanation for the summer $N_m F_2$ disagreement at Poker Flat is that the atomic to molecular density ratio is too low. Independent GUVI observations of the O and N_2 concentrations over Poker in the latter part of July and the beginning of August support this contention.

[37] This research has revealed an interesting peak in electron temperature that occurs in the data and model after sunset in winter months. This feature is attributed to a

combination of a sharp decrease in electron-ion cooling as the electron density rapidly decreases after local sunset in the presence of a slowly decaying topside heat flow.

[38] The FLIP model equivalent winds calculated from the measured $h_m F_2$ also agree well with the radar winds. The IRI model gives a satisfactory fit to the median $h_m F_2$ and $N_m F_2$ data during 2007 and the HWM93 model produces winds that agree well with the radar winds. The HWM07 model winds do not agree as well as HWM93 with the Poker Flat data. We conclude that our understanding of ionospheric processes is satisfactory, although some of the details of individual processes still need further exploration.

[39] **Acknowledgments.** This research was supported by NASA grants NNX07AN03G and NNX08AF43G to George Mason University and the NASA TIMED Program. The Utah State University research was supported through NSF grant ATM-0533543. PFISR data collection and analysis was supported under NSF cooperative agreement ATM-0608577. The Millstone Hill Observatory research was supported by NSF grant ATM0733510.

[40] Wolfgang Baumjohann thanks Joseph Huba and Stephan Buchert for their assistance in evaluating this paper.

References

- Aponte, N., M. J. Nicolls, S. A. Gonzalez, M. P. Sulzer, M. C. Kelley, E. Robles, and C. A. Tepley (2005), Instantaneous electric field measurements and derived neutral winds at Arecibo, *Geophys. Res. Lett.*, *32*, L12107, doi:10.1029/2005GL022609.
- Aponte, N., M. P. Sulzer, M. J. Nicolls, R. Nikoukar, and S. A. Sixto (2007), Molecular ion composition measurements in the F1 region at Arecibo, *J. Geophys. Res.*, *112*, A06322, doi:10.1029/2006JA012028.
- Bilitza, D. (2001), International Reference Ionosphere 2000, *Radio Sci.*, *36*, 261–275, doi:10.1029/2000RS002432.
- Bilitza, D., K. Rawer, L. Bossey, and T. Gulyaev (1993), International reference ionosphere—Past, present, and future, *Adv. Space Res.*, *13*(3), 3–13, doi:10.1016/0273-1177(93)90240-C.
- Buonsanto, M. J., and O. G. Witasse (1999), An updated climatology of thermospheric neutral winds and F region ion drifts above Millstone Hill, *J. Geophys. Res.*, *104*, 24,675–24,687, doi:10.1029/1999JA900345.
- Buonsanto, M. J., D. P. Sipler, G. B. Davenport, and J. M. Holt (1997a), Estimation of the O⁺, O collision frequency from coincident radar and Fabry-Perot observations at Millstone Hill, *J. Geophys. Res.*, *102*, 17,267–17,274, doi:10.1029/97JA01300.
- Buonsanto, M. J., M. J. Starks, J. E. Titheridge, P. G. Richards, and K. L. Miller (1997b), Comparison of techniques for derivation of neutral meridional winds from ionospheric data, *J. Geophys. Res.*, *102*, 14,477–14,484, doi:10.1029/97JA01149.
- Drob, D. P., et al. (2008), An empirical model of the Earth's horizontal wind fields: HWM07, *J. Geophys. Res.*, *113*, A12304, doi:10.1029/2008JA013668.
- Dyson, P. L., T. P. Davies, M. L. Parkinson, A. J. Reeves, P. G. Richards, and C. E. Fairchild (1997), Thermospheric neutral winds at southern mid-latitudes: A comparison of optical and ionosonde $h_m F_2$ methods, *J. Geophys. Res.*, *102*, 27,189–27,196, doi:10.1029/97JA02138.
- Emmert, J. T., R. R. Meier, J. M. Picone, J. L. Lean, and A. B. Christensen (2006), Thermospheric density 2002–2004: TIMED/GUVI dayside limb observations and satellite drag, *J. Geophys. Res.*, *111*, A10S16, doi:10.1029/2005JA011495.
- Evans, J. V., and W. L. Oliver (1972), The study of E-region ion concentration and composition by incoherent scatter radar, *Radio Sci.*, *7*, 103–112, doi:10.1029/RS007i001p00103.
- Fox, J. L., and K. Y. Sung (2001), Solar activity variations of the Venus thermosphere/ionosphere, *J. Geophys. Res.*, *106*, 21,305–21,335, doi:10.1029/2001JA000069.
- Hedin, A. E., et al. (1996), Empirical wind model for the upper, middle, and lower atmosphere, *J. Atmos. Terr. Phys.*, *58*, 1421–1447, doi:10.1016/0021-9169(95)00122-0.
- Heinselman, C. J., and M. J. Nicolls (2008), A Bayesian approach to electric field and E-region neutral wind estimation with the Poker Flat Advanced Modular Incoherent Scatter Radar, *Radio Sci.*, *43*, RS5013, doi:10.1029/2007RS003805.
- Hierl, P. M., I. Dotan, J. V. Seeley, J. M. Van Doren, R. A. Morris, and A. A. Viggiano (1997), Rate constants for the reactions of O⁺ with N₂ and O₂ as a function of temperature (300–1800 K), *J. Chem. Phys.*, *106*(9), 3540, doi:10.1063/1.473450.
- Itikawa, Y. (1975), Electron-ion energy transfer rate, *J. Atmos. Terr. Phys.*, *37*, 1601–1602, doi:10.1016/0021-9169(75)90041-0.
- Li, X., Y. L. Huang, G. D. Flesch, and C. Y. Ng (1997), A state-selected study of the ion-molecule reactions O⁺(⁴S, ²D, ²P) + N₂, *J. Chem. Phys.*, *106*, 1373, doi:10.1063/1.474087.
- McFarland, M., D. L. Albritton, F. C. Fehsenfeld, E. E. Ferguson, and A. L. Schmeltekopf (1973), Flow-drift technique for ion mobility and ion-molecule reaction rate constant measurements. II. Positive ion reactions of N⁺, O⁺, and H₃⁺ with O₂ and O⁺ with N₂ from thermal to ~2 eV, *J. Chem. Phys.*, *59*, 6620, doi:10.1063/1.1680042.
- Oliver, W. L. (1975), Models of F1-region composition variations, *J. Atmos. Terr. Phys.*, *37*, 1065–1076, doi:10.1016/0021-9169(75)90152-X.
- Richards, P. G. (1986), Thermal electron quenching of N(²D): Consequences for the ionospheric photoelectron flux and the thermal electron temperature, *Planet. Space Sci.*, *34*, 689–694, doi:10.1016/0032-0633(86)90123-6.
- Richards, P. G. (1991), An improved algorithm for determining neutral winds from the height of the F₂ peak electron density, *J. Geophys. Res.*, *96*, 17,839–17,846, doi:10.1029/91JA01467.
- Richards, P. G. (2001), Seasonal and solar cycle variations of the ionospheric peak electron density: Comparison of measurement and models, *J. Geophys. Res.*, *106*, 12,803–12,819, doi:10.1029/2000JA000365.
- Richards, P. G. (2002), Ion and neutral density variations during ionospheric storms in September 1974: Comparison of measurement and models, *J. Geophys. Res.*, *107*(A11), 1361, doi:10.1029/2002JA009278.
- Richards, P. G. (2004), On the increases in nitric oxide density at midlatitudes during Ionospheric Storms, *J. Geophys. Res.*, *109*, A06304, doi:10.1029/2003JA010110.
- Richards, P. G., J. A. Fennelly, and D. G. Torr (1994), EUVAC: A solar EUV flux model for aeronomic calculations, *J. Geophys. Res.*, *99*, 8981–8992, doi:10.1029/94JA00518.
- Richards, P. G., et al. (2000), On the relative importance of convection and temperature on the behavior of the ionosphere in North America during January 6–12, 1997, *J. Geophys. Res.*, *105*, 12,763–12,776, doi:10.1029/1999JA000253.
- Richards, P. G., T. N. Woods, and W. K. Peterson (2006), HEUVAC: A new high resolution solar EUV proxy model, *Adv. Space Res.*, *37*(2), 315–322, doi:10.1016/j.asr.2005.06.031.
- Salah, J. E. (1993), Interim standard for the ion-neutral atomic oxygen collision frequency, *Geophys. Res. Lett.*, *20*, 1543–1546, doi:10.1029/93GL01699.
- Salah, J. E., and J. M. Holt (1974), Midlatitude thermospheric winds from incoherent scatter radar and theory, *Radio Sci.*, *9*, 301–313, doi:10.1029/RS009i002p00301.
- Schunk, R. W., and A. F. Nagy (1978), Electron temperatures in the F region of the ionosphere: Theory and observations, *Rev. Geophys.*, *16*, 355–399, doi:10.1029/RG016i003p00355.
- Schunk, R. W., and J. C. G. Walker (1973), Theoretical ion densities in the lower ionosphere, *Planet. Space Sci.*, *21*, 1875–1896, doi:10.1016/0032-0633(73)90118-9.
- Sojka, J. J., M. J. Nicolls, C. J. Heinselman, and J. D. Kelly (2009), The PFISR IPY observations of ionospheric climate and weather, *J. Atmos. Sol. Terr. Phys.*, *71*, 771–785, doi:10.1016/j.jastp.2009.01.001.
- St.-Maurice, J.-P., and D. G. Torr (1978), Nonthermal rate coefficients in the ionosphere: The reactions of O⁺ with N₂, O₂, and NO, *J. Geophys. Res.*, *83*(A3), 969–977, doi:10.1029/JA083iA03p00969.
- Woods, T. N., et al. (2008), XUV photometer system (XPS): Improved solar irradiance algorithm using CHIANTI spectral models, *Sol. Phys.*, *250*, 235–267, doi:10.1007/s11207-008-9196-6.

C. J. Heinselman and M. J. Nicolls, Center for Geospace Studies, SRI International, 333 Ravenswood Ave., Menlo Park, CA 94025, USA.

J. M. Holt, Haystack Observatory, Massachusetts Institute of Technology, Rte. 40, Westford, MA 01886, USA.

R. R. Meier and P. G. Richards, Department of Physics and Astronomy, George Mason University, Fairfax, VA 22030, USA. (pricharl@gmu.edu)

J. J. Sojka, Center for Atmospheric and Space Sciences, Utah State University, Logan, UT 84322-4405, USA.